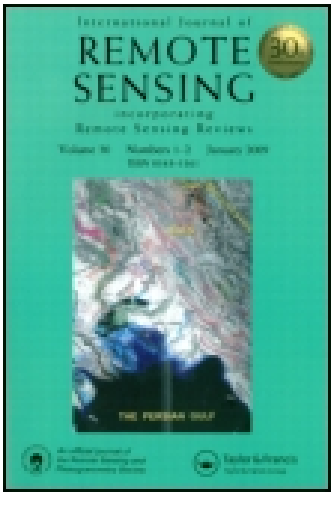

International Journal of Remote Sensing
Publication details, including instructions for authors and subscription information:
http://www.tandfonline.com/loi/tres20

A new band ratio technique for mapping debris-covered glaciers using Landsat imagery and a digital elevation model

Haireti Alifu[a], Ryutaro Tateishi[b] & Brian Johnson[c]
[a] Geosystem and Biological Sciences Division, Graduate Schools of Science, Chiba University, Inage-ku, Chiba-shi, Chiba, Japan
[b] Centre for Environmental Remote Sensing, Chiba University, Inage-ku, Chiba-shi, Chiba, Japan
[c] Institute for Global Environmental Strategies (IGES), Hayama, Kanagawa, Japan
Published online: 20 Apr 2015.

To cite this article: Haireti Alifu, Ryutaro Tateishi & Brian Johnson (2015) A new band ratio technique for mapping debris-covered glaciers using Landsat imagery and a digital elevation model, International Journal of Remote Sensing, 36:8, 2063-2075

To link to this article: http://dx.doi.org/10.1080/2150704X.2015.1034886

International Journal of Remote Sensing, 2015
Vol. 36, No. 8, 2063–2075, http://dx.doi.org/10.1080/2150704X.2015.1034886

Taylor & Francis
Taylor & Francis Group

A new band ratio technique for mapping debris-covered glaciers using Landsat imagery and a digital elevation model

Haireti Alifu [a]*, Ryutaro Tateishi[b], and Brian Johnson[c]

[a]*Geosystem and Biological Sciences Division, Graduate Schools of Science, Chiba University, Inage-ku, Chiba-shi, Chiba, Japan;* [b]*Centre for Environmental Remote Sensing, Chiba University, Inage-ku, Chiba-shi, Chiba, Japan;* [c]*Institute for Global Environmental Strategies (IGES), Hayama, Kanagawa, Japan*

(*Received 18 December 2014; accepted 20 March 2015*)

Mapping of debris-covered glaciers using optical remote-sensing data is a difficult task due to the fact that the debris cover on the glacier surface has a similar reflectance to surrounding rocky or sandy areas in the visible to near-infrared wavelength region. Therefore, a new method was developed for mapping debris-covered glaciers that considers thermal and slope information in addition to visible and near-infrared information. The method was tested for delineating the Koxkar glacier and Yengisogat glacier using Landsat Enhanced Thematic Mapper Plus and Landsat Thematic Mapper imagery and Shuttle Radar Topography Mapping Mission (SRTM) data. Specifically, the method combines a new band ratio image with slope information derived from the SRTM digital elevation model to better distinguish periglacial debris and supraglacial debris. The new band ratio image considers the near infrared (NIR), shortwave infrared (SWIR), and thermal infrared (TIR) bands, and is given by TIR/(NIR/SWIR). The debris-covered glacier boundaries are generated by thresholding the new band ratio image and overlaying it onto a binary slope map. Accuracy assessment was carried out through comparisons of the classified maps with reference maps from the Randolph Glacier Inventory, Glacier Inventory GIS data of China, and a manual delineation done using Google Earth™ images. The accuracy assessment shows that the result from the proposed method has a good agreement with the different reference data sets.

1. Introduction

Glaciers are considered as key indicators of climate change due to their sensitive reaction to even small climatic changes (Lemke et al. 2007). Changes in temperature, precipitation, and other climate factors can cause changes in glaciers' physical properties (Ranzi et al. 2004; Haeberli et al. 2007). Hence, glaciers can provide local climate change information, especially in areas where climate stations are rare. Glaciers are also very important freshwater resources in many arid and semi-arid regions. Therefore, mapping, monitoring, and inventory of glaciers are important for assessing the impacts of climate change (Shukla, Gupta, and Arora 2010) and management of water resources (Bajracharya and Mool 2010). However, detailed glacier inventory data are still lacking in most parts of the world (IPCC 2007). Remote-sensing imagery is the only effective tool for repetitive glacier monitoring due to the extremely unstable and inaccessible terrain as well as the harsh weather conditions of many large glaciers in high mountainous regions. Several

*Corresponding author. Email: acxa3412@chiba-u.jp

automated and semi-automatic remote-sensing techniques have been developed and tested for mapping clean glacier ice with good accuracy, as reported in previous studies (Racoviteanu et al. 2009; Bhambri and Bolch 2009; Paul et al. 2013). However, these methods fail when applied to debris-covered glaciers because supraglacial debris (debris cover on the glacier) and periglacial debris (debris cover on the outside the glacier margin) have a similar spectral response (since they both are derived from the valley rock materials).

Therefore, various techniques have been developed for mapping debris-covered glaciers using optical remote-sensing data. They can be summarized into several categories: (i) manual delineation methods (Paul et al. 2002), (ii) multispectral image classification methods (Bishop, Hickman, and Shroder 1999), (iii) thermal-properties-based methods (Taschner and Ranzi 2002; Ranzi et al. 2004), (iv) geomorphometric-parameters-based methods (Bishop et al. 2001; Bolch and Kamp 2006), and (v) methods which use a combination of the above-mentioned methods (Paul, Huggel, and Kääb 2004; Keshri, Shukla, and Gupta 2009; Shukla, Gupta, and Arora 2010; Shukla, Arora, and Gupta 2010; Bhambri, Bolch, and Chaujar 2011). The manual delineation method is generally considered as accurate, but it is time consuming and its accuracy depends on the image quality and the interpreter's ability to identify the debris cover on the glacier terrain features. As for multispectral image classification methods, Bishop, Hickman, and Shroder (1999) applied an artificial neural network classifier for detecting debris-covered glaciers in the Himalaya region, but the longer processing time may limit its applicability over large regions (Racoviteanu et al. 2009). Thermal properties-based methods are based on the temperature difference that exists between the supraglacial debris and the periglacial debris region. However, this method cannot detect the debris-covered glaciers when the debris layer is thicker than 40–50 cm (Taschner and Ranzi 2002; Ranzi et al. 2004). The geomorphometric-based method fails at mapping a debris-covered glacier when the glacier tongue transition to the unglaciated region is gentle (Bolch and Kamp 2006). In summary, all of these previous approaches (including the combined approaches) have difficulty when applied for (a) mapping debris-covered glaciers covered by a thick debris layer and/or (b) mapping debris-covered glaciers when the glacier terminus region transition to the unglaciated region is gentle (Bolch and Kamp 2006; Bolch et al. 2008; Bhambri, Bolch, and Chaujar 2011).

Therefore, in this study, in an attempt to solve the above problems, we developed a new approach that combines a new band ratio technique with slope information to delineate debris-covered glaciers. We tested the proposed method for mapping the boundary of Koxkar glacier (41° 45′ 36.00″ N, 80° 6′ 36.00″ E, Figure 1(*a*)) in northwestern China and the Yengisogat glacier (36° 4′ 58.80″ N, 76° 6′ 10.08″ E, Figure 1(*b*)), located in the northern slopes of the Chinese Karakoram mountain range.

The Koxkar glacier is 25.1 km long and covers an area of 83.56 km^2 (Han et al. 2010). It has a gentle terminus region (Liu, Mayer, and Liu 2013) and is covered by a thick debris layer in the ablation region (Juen et al. 2014). The Yengisogat glacier is a valley glacier, it has four branches, is 42 km long with an area of 379.97 km^2, and has an ice volume of 115.89 km^3 (according to the Glacier Inventory of China in the 1970s; Shi, Liu, and Wang 2008). The transition from the terminus of the Yengisogat glacier to the unglaciated region is gentle (Figure 1(*c*)) and covered by a thick debris layer (Shi, Liu, and Wang 2008). Thus, these two are considered as good test areas for examination of our method.

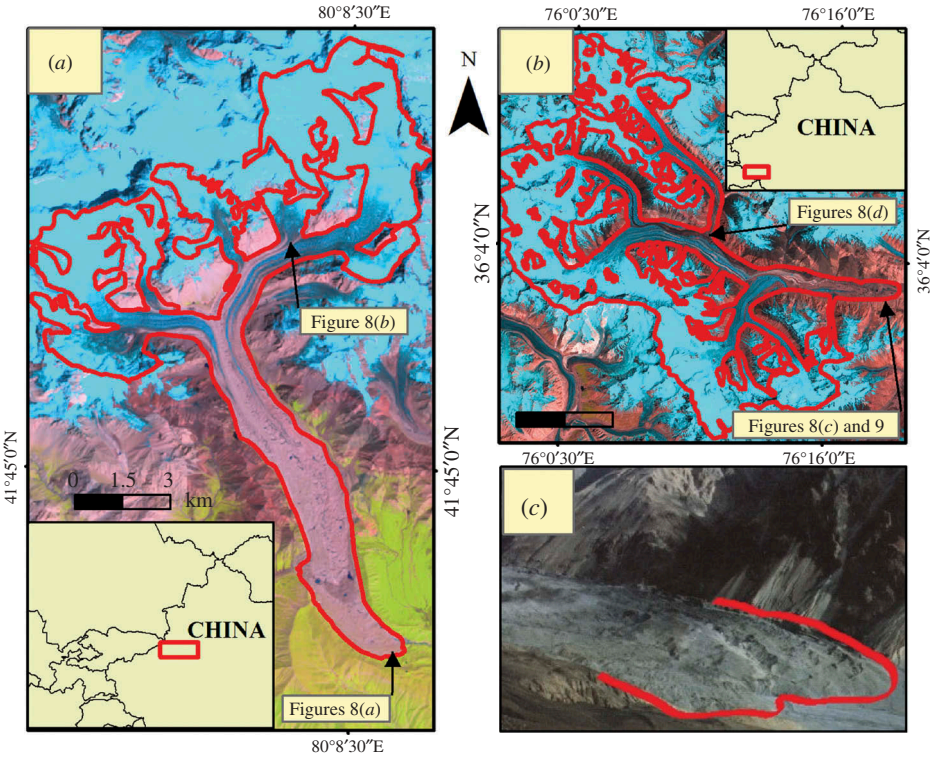

Figure 1. (*a*) Koxkar glacier with glacier outline (red line) from the Randolph Glacier Inventory. (*b*) Yengisogat glacier with glacier outline (red line) from the Glacier Inventory of China. Landsat images are false colour composites with R = shortwave infrared band, G = red band, B = green band. (*c*) Yengisogat glacier tongue (red), taken by John Shen in April, 2003 (image source: http://www.summitpost.org/mount-crown-huangguan/152162).

2. Data

2.1. Data used for glacier mapping

For this study, a Landsat-5 Thematic Mapper (TM) image (acquisition date: 4 August 2009, Figure 1(*b*)) was used for mapping the Yengisogat glacier and a Landsat-7 Enhanced Thematic Mapper Plus (ETM+) image (acquisition date: 31 July 2013, Figure 1(*a*)) was used for mapping the Koxkar glacier due to the similar acquisition dates of these Landsat images and the available reference data sets/free high-resolution Google Earth™ images of the glaciers. The Landsat images were both acquired at the end of the summer season, and no seasonal snow or cloud cover was present in the scenes. The Landsat images were downloaded from USGS EarthExplorer (USGS EE; http://earthexplorer.usgs.gov/). Landsat-5 (TM) has seven bands. Six bands in the visible to shortwave infrared (SWIR) region have a spatial resolution of 30 m and one thermal infrared (TIR) band has a 120 m spatial resolution. Landsat-7 ETM+ has eight multi-spectral bands, with six visible to SWIR bands of 30 m spatial resolution, two TIR bands of 60 m resolution and one panchromatic band of 15 m resolution. The Koxkar glacier was situated in the centre (gap-free area) of the Landsat ETM+ footprint, enabling us to use the imagery despite the scan-line correction failure (Figure 1(*a*)).

A Shuttle Radar Topography Mission (SRTM) digital elevation model (DEM) was used for deriving the slope information. Previously, SRTM data for regions outside the USA were provided at 90 m resolution, but on 2 January 2015, SRTM version 3.0 (SRTMV3) with 30 m resolution was released for Asia. SRTM (90 m and 30 m) resolution data were freely download form NASA's Earth System Data and Information System (http://reverb.echo.nasa.gov/). The 90 m-resolution SRTM data were used for extracting the slope information of the Yengisogat glacier (since our analysis of this glacier was done prior to January 2015), and the 30 m resolution SRTM data was downloaded to extract the slope information of the Koxkar glacier.

2.2. *Reference data sets*

Glacier inventory data and manual delineations of the glaciers from high-resolution Google Earth™ images were used to validate the results of this study. Google Earth™ images with similar dates to the Landsat images were used for the manual glacier delineation. Google Earth™ images from 22 August 2009, 9 September 2009, 30 September 2009 and 30 October 2009 were used for delineating the Yengisogat glacier, and Google Earth™ images from 29 January 2013 and 29 July 2013 were used for delineating the Koxkar glacier.

The Glacier Inventory of China 2009 (GIC 2009) data set was also used as reference data for the Yengisogat glacier. This data set is provided by 'Investigation on glacier resources and their change in China' (2006FY110200) and 'Glacier change monitoring and its impact assessment research in west China' (:kzcx2-yw-301) (http://westdc.westgis.ac.cn/glacier), and the Yengisogat glacier outline in the data set was extracted from Landsat series imagery and then manually corrected using ASTER images, old topographic maps, and Google Earth™ images (Liu et al. 2015).

The Randolph Glacier Inventory (RGI) was used as a second reference data set for the Koxkar glacier. RGI is a collection of digital outlines of the world's glaciers, excluding the Greenland and Antarctic ice sheets (Pfeffer et al. 2014). The RGI version 4.0 (RGI V4) was freely downloaded from the Global Land Ice Measurements from Space website (http://www.glims.org/RGI/index.html). The glacier outlines in these reference sets showed good agreement compared to our manually delineated glacier boundaries.

3. Methods

3.1. *Generating the new band ratio image*

Clean glacier ice has a high reflectivity in the visible to near-infrared wavelengths (0.4–1.2 μm) and a very low reflectivity in the SWIR wavelength region (1.4–2.5 μm). The commonly used band ratio images consider Landsat TM or ETM+ bands 2 (green), 3 (red), 4 (NIR) and 5 (SWIR) to take advantage of these spectral differences at different wavelengths and separate clean glacier ice from non-glacier surfaces, for example, band 3/band 5 (Andreassen et al. 2008), band 4/band 5 (Paul et al. 2002), and the normalized difference snow index ((band 2 – band 5)/(band 2 + band 5)) (Silverio and Jaquet 2005) (TM and ETM+ band numbers are the same in these equations). While clean glacier ice has high values in these ratio images, supraglacial debris and other nearby non-glacier rocky surfaces have low values because the supraglacial debris and the other rocky surfaces have similar spectral responses at these wavelengths. On the other hand, the TIR band (band 6 of TM and ETM+) can provide information on the temperature

difference of different surfaces, which can help to separate the supraglacial debris from other rock materials. Temperature data from field measurements as well as from remote-sensing techniques have indicated that supraglacial debris areas have significantly lower surface temperatures than periglacial debris areas (Taschner and Ranzi 2002; Ranzi et al. 2004; Shukla, Gupta, and Arora 2010; Shukla, Arora, and Gupta 2010; Karimi et al. 2012). Thus, the idea for our new band ratio technique comes out of these characteristics. Low values of supraglacial debris in the band 4/band 5 image (Figures 2(*c*) and 3(*c*)) allow it to be separated from periglacial debris when the Landsat thermal band (band 6, Figures 2(*b*) and 3(*b*)) is divided by the result of band 4/band 5 (Figures 2(*d*) and 3(*d*)). In this study, we derived the new band ratio image (Equation (1)) by dividing digital number (DN) values of the thermal band (band 6) by the DN value of band 4 divided by band 5:

$$\text{New band ratio} = \text{band } 6 \div (\text{band } 4 \div \text{band } 5). \tag{1}$$

As shown in Figures 2(*d*) and 3(*d*), compared with the conventional band ratio technique, in the new band ratio technique the supraglacial debris areas (light grey areas) are more distinct from the surrounding non-glacier areas.

Next, the glaciers were classified by thresholding the new band ratio imagery. Here, the density slicing method was used to select the threshold ranges for glacier mapping (Meier 1980). The density slicing method is useful when a given surface feature has a unique and generally narrow set of DN values (Short 1999). If several features each have different (separable) DN values, then several level slices may be produced, each mapping

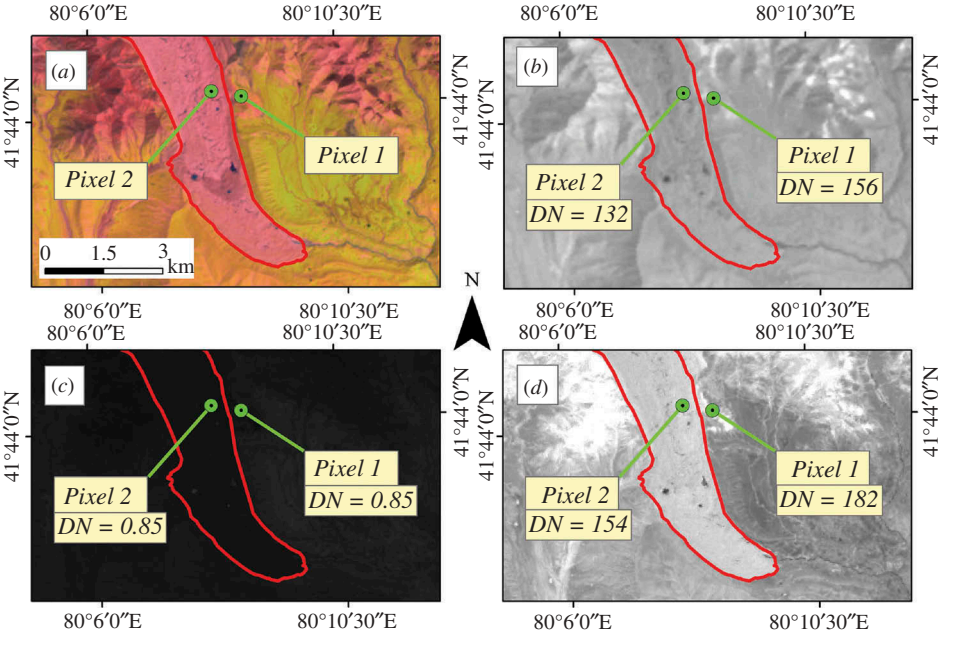

Figure 2. (*a*) Koxkar glacier terminus region and location of pixel 1 (periglacial debris region) and pixel 2 (supraglacial debris region) in a false colour composite image (band combination, R = shortwave infrared band, G = red band, B = green band). (*b*) Koxkar glacier terminus region in the thermal band (band 6_1). (*c*) Band ratio image using the previous method (band 4/band 5). (*d*) Proposed band ratio image. Koxkar glacier outline (red line) from the Randolph Glacier Inventory.

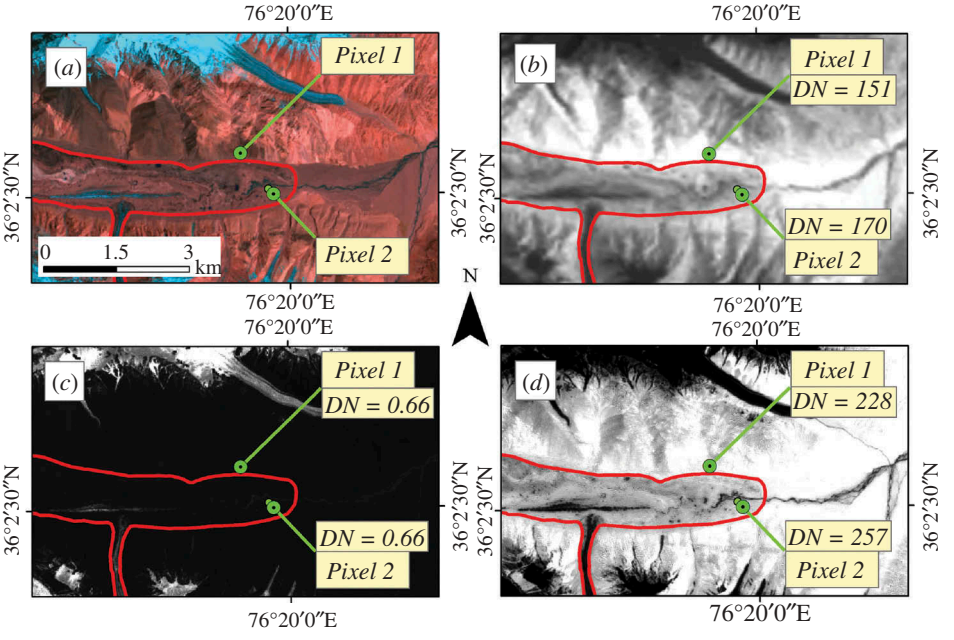

Figure 3. Yengisogat glacier terminus region and location of pixel 1 (periglacial debris region) and pixel 2 (supraglacial debris region) in (*a*) a false colour composite (R = shortwave infrared band, G = red band, B = green band). (*b*) Thermal band (band 6). (*c*) Band ratio image using the previous method (band 4/band 5). (*d*) Proposed band ratio image. Yengisogat glacier outline (red line) from the Glacier Inventory of China.

the spatial distribution of its corresponding feature (Short 1999). All pixels within a 'slice' (i.e. a range) of pixel values are considered to belong to the same information class (i.e. 'clean glacier ice', 'supraglacial debris', and 'other classes'). The result of the density slice, shown in Figures 4(*b*) and 5(*b*), contained several inaccuracies for the 'supraglacial debris' class in areas where bedrock valley walls were located in shade and/or in higher elevation areas (e.g. Figures 4(*i*), (*ii*) and 5(*i*), (*ii*)). The bedrock valley walls in shade area may have lower temperature than illuminated areas and also spectral information of rocky materials was reduced. Especially, periglacial debris regions near the accumulation zone have low temperatures due to their locations at higher elevations. However, we found that these classification errors could be eliminated when slope information was also considered.

3.2. Delineating the final debris-covered glacier boundary by combining the classified map with slope information

In this study, a slope raster image was generated from the SRTM DEM data. Previous studies combined morphometric parameters such as slope with other information to delineate the debris-covered glacier boundary (Bishop et al. 2001; Paul, Huggel, and Kääb 2004; Bolch and Kamp 2006; Shukla, Arora, and Gupta 2010; Bhambri, Bolch, and Chaujar 2011). Bishop et al. (2001) show that mean of the slope is a key parameter to delineate debris-covered glaciers. In this study, a slope threshold value of less than 12° was selected based on visual evaluation to create a binary slope map for both test areas

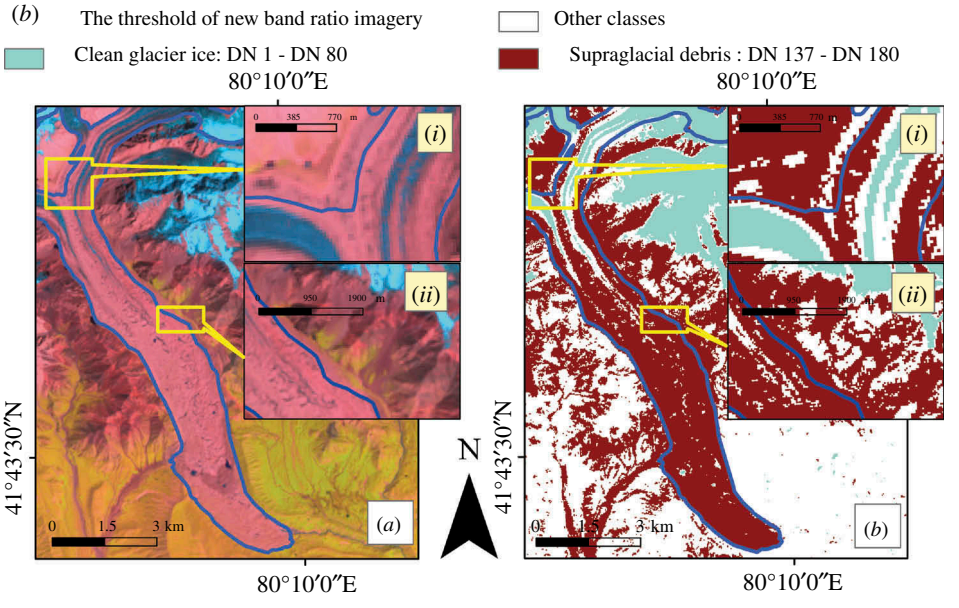

Figure 4. (*a*) Koxkar glacier ablation region. (*b*) Thresholding range of the new band ratio image using the density slicing method. (*i*) and (*ii*) Closer view of the misclassified periglacial debris region. Koxkar glacier outline (blue line) from the Randolph Glacier Inventory.

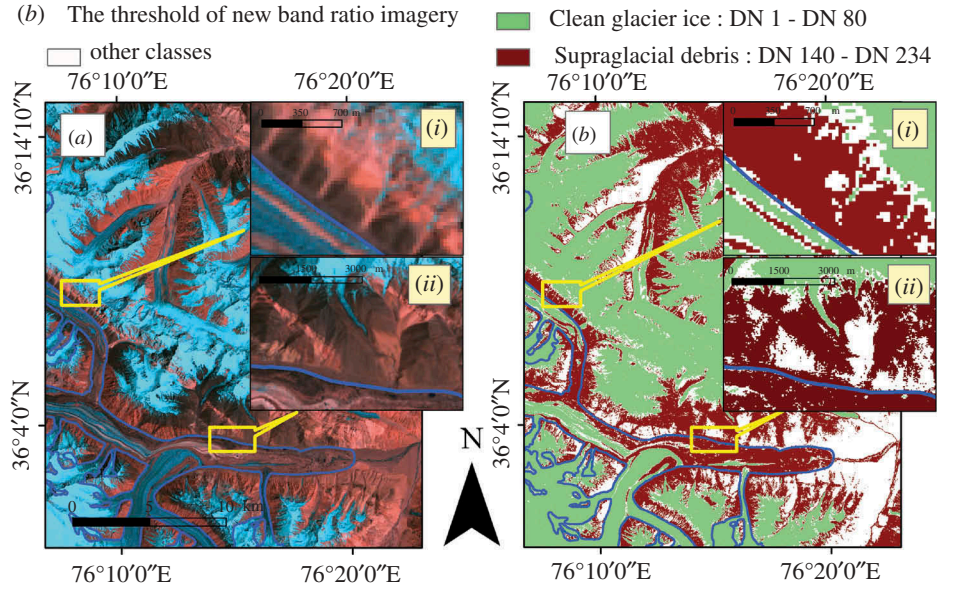

Figure 5. (*a*) Yengisogat glacier ablation region. (*b*) Thresholding of the new band ratio image using the density slicing method. (*i*) and (*ii*) Closer view of the misclassified periglacial debris region. Yengisogat glacier outline (blue line) from the Glacier Inventory of China.

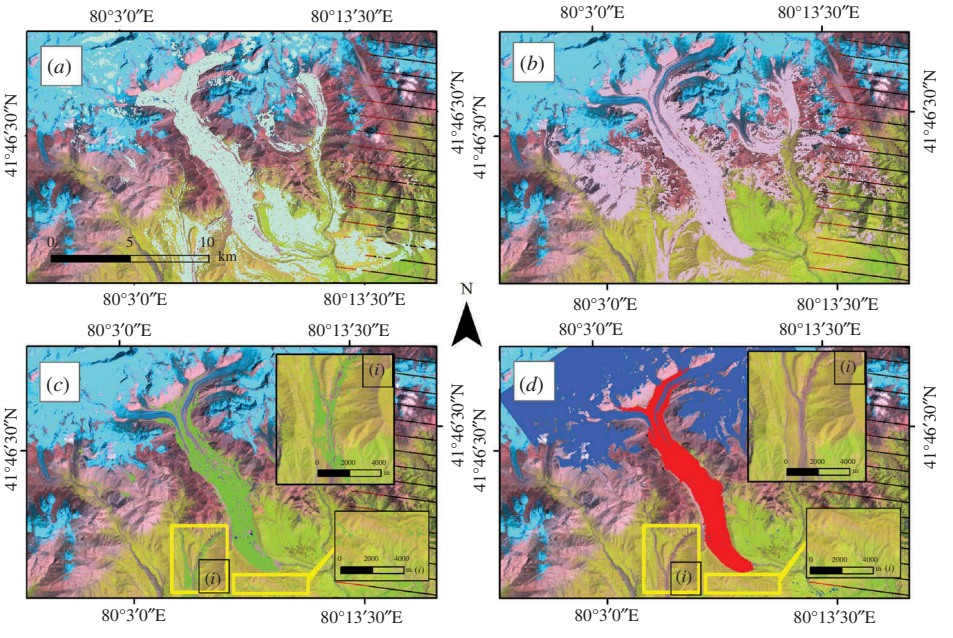

Figure 6. (*a*) Binary slope (<12°) map. (*b*) Map derived from the thresholding the new band ratio image. (*c*) Map of supraglacial debris derived from the intersection of map (*a*) and map (*b*). (*d*) Map showing areas of supraglacial debris (in red) merged with those of clean glacier ice (in blue). (*i*) Closer view of an area of some vegetation that needed to be manually removed.

(Figures 6(*a*) and 7(*a*)). The debris is transported by general down-slope movement of a glacier towards the terminus (if local surface slope is too steep, debris usually slides farther down until a more gentle slope allows accumulation) (Paul, Huggel, and Kääb 2004). Therefore, glacier gradient information can be used to eliminate the other bedrock valley walls.

The DN values in the new band ratio image from 137 to 180 (Figures 4(*b*) and 6(*b*)) and 140 to 234 (Figures 5(*b*) and 7(*b*)) were used as the thresholds for mapping the supraglacial debris areas in the Koxkar glacier and Yengisogat glaciers, respectively. The thresholded result was overlaid onto the binary slope map, as shown in Figures 6(*c*) and 7 (*c*). Some areas, such as river channels (Figure 7(*c*) (*i*)) which are connected with glacier tongue and vegetation areas (Figure 6(*c*) (*i*)), needed to be manually removed. Final debris-covered glacier boundaries were generated by combining the result from the supraglacial debris map with clean glacier ice maps derived using threshold values DN ranging from 1 to 80 for both glaciers (Figures 4(*b*) and 5(*b*) with green, and Figures 6(*d*) and 7(*d*) with blue).

4. Accuracy assessment

The RGI 4V, GIC 2009 and manual delineations of the high-resolution Google Earth™ images were used to evaluate the result from this study. Specifically, the areas of the Koxkar glacier (Figures 8(*a*) and (*b*)) and Yengisogat glacier (Figures 8(*c*) and (*d*)) in the reference maps were compared with the areas of the glaciers calculated using the proposed

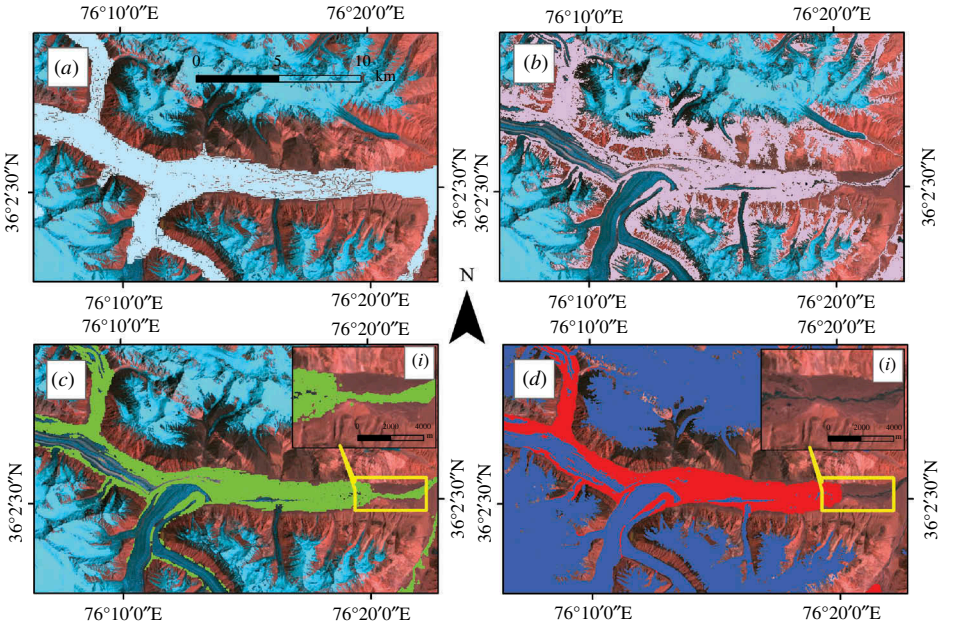

Figure 7. (*a*) Binary slope (<12°) map. (*b*) Map derived from thresholding the new band ratio image. (*c*) Map of supraglacial debris derived from the intersection of map (*a*) and map (*b*). (*d*) Map showing areas of supraglacial debris (in red) merged with those of clean glacier ice (in blue). (*i*) Closer view of some river channel that needed to be manually removed.

methods. All of the vector maps of the glaciers were overlaid onto Google Earth™ images to allow for a visual comparison (Figure 8).

5. Results and discussion

The accuracy assessment showed that the glacier boundary derived from the combination of the new band ratio image with the binary slope image was quite similar to the inventory data (Figure 8). Specifically, there was a 0.34% difference between the Koxkar glacier area measurement from the proposed method (62.607 km^2) and the RGI V4 measurement (62.821 km^2), and a 2% difference compared with the manual delineation (63.886 km^2). For the Yengisogat glacier, there was a 2% difference between the glacier area measurements from the proposed method (362.1 km^2) and the reference data sets (359.05 and 363.92 km^2). However, as shown in Figure 8(*d*), the Yengisogat glacier extent produced by our method was slightly overestimated in some supraglacial areas. This was likely because the spatial resolutions of the SRTM data (90 m resolution) and Landsat TM thermal band (120 m resolution) were not high enough to reflect the complicated glacier terrain features. Therefore, some manual editing was required to improve the result.

Selecting the threshold values is a critical step for delineating the debris-covered glacier accurately, but the threshold values were shown to differ from glacier to glacier. Therefore, the thresholds should be selected carefully by overlaying the density-sliced maps with Landsat composite images and other ancillary data (e.g. high-resolution Google Earth™ images, if available). The threshold values used in this study were selected because they clearly separated the supraglacial debris and the unglaciated area in the

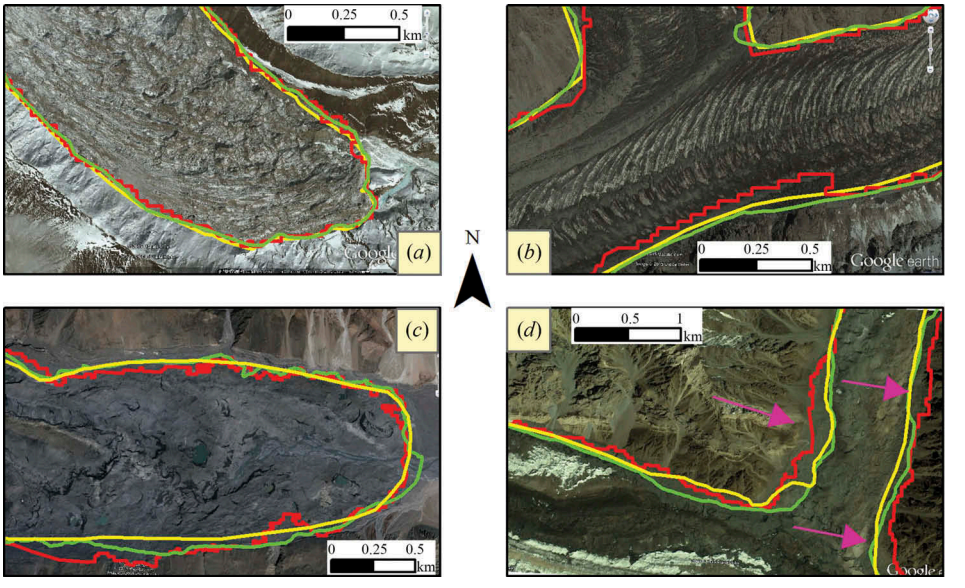

Figure 8. Comparison of the results for the delineation of the Koxkar glacier (*a* and *b*) and Yengisogat glacier (*c* and *d*) using the different methods described in this paper. (*a*) and (*b*) Yellow = Koxkar glacier boundary according to the Randolph Glacier Inventory, red = Koxkar glacier boundary based on the result of this study, green = Koxkar glacier boundary manually delineated from Google Earth™ images. (*c*) and (*d*) Yellow = Yengisogat glacier boundary according to the Glacier Inventory of China, red = Yengisogat glacier boundary based on the result of this study, green = Yengisogat glacier boundary manually delineated from Google Earth™ images, pink point mark shows the overestimated supraglacial debris area. Images: screenshots from Google Earth™. Image dates: (*a*) 29 January 2013, (*b*) 29 July 2013, (*c*) 9 September 2009 and (*d*) 30 September 2009.

glacier terminus region. Due to fact that most glacier slope facets differ from each other, the slope threshold values may also need to be modified to apply our method to other glaciers (a slope threshold value which can reflect the glacier's terrain would be needed).

The previous glacier mapping methods failed when applied to glaciers covered by thick debris and/or when the glacier terminus region transition to the unglaciated region was gentle (Bishop et al. 2001; Taschner and Ranzi 2002; Ranzi et al. 2004; Bolch and Kamp 2006; Bolch et al. 2008). Shukla, Gupta, and Arora (2010) and Shukla, Arora, and Gupta (2010) integrated optical data (the Indian Remote Sensing satellite – Resourcesat-1's Advanced Wide Field Sensor) and thermal data (ASTER) to successfully map the Samudra Tapu glacier in the Himalaya region. However, the requirement of cloud-free images for both of these data sets may decrease the method's practical applicability to wide regions. Another combined approach, developed by Paul, Huggel, and Kääb (2004), failed when transferred to the Himalayan debris-covered glaciers (Shukla, Arora, and Gupta 2010). As an example of the limitations of existing combined approaches in one of our areas of interest (Yengisogat glacier), Alifu and Tateishi (2013) applied the approach from Bhambri, Bolch, and Chaujar (2011) (clustering result of slope, plan curvature and profile curvature combined with thermal mask and a band 4/band 5 ratio image) to map the glaciers in the Shaksgam valley of the Chinese Korakoram mountain region, but the Yengisogat glacier terminus region was not able to be mapped using that approach

Figure 9. Comparison of the results from Alifu and Tateishi (2013) and method described in this paper. Yengisogat glacier boundary based on the result of this study (red), Yengisogat glacier boundary based on the result from Alifu and Tateishi (2013) (pink). Image: screenshots from Google Earth™. Image date: 9 September 2009.

(Figure 9). The semi-automated method developed in this study used free satellite data and was able to map thick debris-covered glaciers with relatively higher accuracy.

6. Conclusions

The proposed method, which involved combining a new band ratio image with slope information, was able to successfully delineate the Koxkar glacier and Yengisogat glacier in this study (only 0.34–2% discrepancy between the mapped glaciers' areas and the reference glaciers' areas). However, the coarse resolution of the thermal band could not separate the spectrally similar supraglacial and periglacial debris in some shaded and/or high-elevation areas. Therefore, additional information from geomorphometric parameters (i.e. slope) was integrated with new band ratio imagery. The result of the approach is promising to map the glaciers in our study areas. However, the supraglacial debris area of Yengisogat glacier was overestimated (Figure 8(*d*), pink point mark) because the SRTM data (90 m resolution) was not good enough to reflect the gradient information from the periglacial debris region to the supraglacial debris region. Hence, manual editing was required to improve the result. The result of the Koxkar glacier outline shows that the 30 m resolution of SRTM V3 data allowed for higher accuracy than the previous SRTM (90 m). The advantage of this multisource combination approach is the semi-automatic processing, which is based on simple characteristics (thermal and spectral). For mapping debris-covered glaciers, the proposed method was similar in terms of accuracy and faster than manual delineation, despite the final manual editing still required. However, the inclusion of additional information, such as more morphometric parameters (e.g. plan curvature and profile curvature) may further improve the accuracy of the debris-covered glacier mapping and allow the method to be applied to large glaciated regions.

Disclosure statement

No potential conflict of interest was reported by the authors.

ORCID

Haireti Alifu http://orcid.org/0000-0002-7369-6657

References

Alifu, H., and R. Tateishi. 2013. "Mapping Glaciers in the Shaksgam Valley Using Landsat TM and ASTER GDEM V2." In *Proceeding of the 55th Autumn Conference of the Remote Sensing Society of Japan*, November 21–22, Japan, 135–136. Nohon University.

Andreassen, L. M., F. Paul, A. Kääb, and J. E. Hausberg. 2008. "Landsat Derived Glacier Inventory for Jotunheimen, Norway, and Deduced Glacier Changes since the 1930s." *The Cryosphere* 2 (2): 131–145. doi:10.5194/tc-2-131-2008.

Bajracharya, S. R., and P. Mool. 2010. "Glaciers, Glacial Lakes and Glacial Lake Outburst Floods in the Mount Everest Region, Nepal." *Annals of Glaciology* 50 (53): 81–86. doi:10.3189/172756410790595895.

Bhambri, R., and T. Bolch. 2009. "Glacier Mapping: A Review with Special Reference to the Indian Himalayas." *Progress in Physical Geography* 33 (5): 672–704. doi:10.1177/0309133309348112.

Bhambri, R., T. Bolch, and R. K. Chaujar. 2011. "Mapping of Debris-Covered Glaciers in the Garhwal Himalayas Using ASTER Dems and Thermal Data." *International Journal of Remote Sensing* 32 (23): 8095–8119. doi:10.1080/01431161.2010.532821.

Bishop, M. P., R. Bonk, U. Kamp, and J. F. Shroder Jr. 2001. "Terrain Analysis and Data Modeling for Alpine Glacier Mapping." *Polar Geography* 25: 182–201. doi:10.1080/10889370109377712.

Bishop, M. P., B. L. Hickman, and J. F. Shroder Jr. 1999. "High Resolution Satellite Imagery and Neural Networks for Information Extraction in a Complex Mountain Environment." *Geocarto International* 14 (2): 17–26. doi:10.1080/10106049908542100.

Bolch, T., M. F. Buchroithner, A. Kunert, and U. Kamp. 2008. "Automated Delineation of Debris-Covered Glaciers Based on ASTER Data." In *Geoinformation in Europe (Proceedings of the 27th Earsel-Symposium, 4.-7.6.07, Bozen, Italy)*, edited by M. A. Gomarasca, 403−410. Rotterdam: Millpress.

Bolch, T., and U. Kamp. 2006. "Glacier Mapping in High Mountains Using Dems, Landsat and ASTER Data." *In Proceedings of the 8th International Symposium on High Mountain Remote Sensing Cartography*, March 20–27, 2005, La Paz, 13–24. Graz: Grazer Schriften de Georaphie und Raumforschung.

Haeberli, W., M. Hoelzle, F. Paul, and M. Zemp. 2007. "Integrated Monitoring of Mountain Glaciers as Key Indicators of Global Climate Change: The European Alps." *Annals of Glaciology* 46 (1): 150–160. doi:10.3189/172756407782871512.

Han, H., J. Wang, J. Wei, and S. Liu. 2010. "Backwasting Rate on Debris-Covered Koxkar Glacier, Tuomuer Mountain, China." *Journal of Glaciology* 56 (196): 287–296. doi:10.3189/002214310791968430.

IPCC (Intergovernmental Panel on Climate Change). 2007. *Climate Change 2007: The Physical Science Basis. Contribution of Working Group I to the Fourth Assessment Report of the Intergovernmental Panel on Climate Change*, 996. Edited by S. Solomon, D. Qin, M. Manning, Z. Chen, M. Marquis, K. B. Averyt, M. Tignor, and H. L. Miller. Cambridge: Cambridge University Press.

Juen, M., C. Mayer, A. Lambrecht, H. Han, and S. Liu. 2014. "Impact of Varying Debris Cover Thickness on Ablation: A Case Study for Koxkar Glacier in the Tien Shan." *The Cryosphere* 8 (2): 377–386. doi:10.5194/tc-8-377-2014.

Karimi, N., A. Farokhnia, L. Karimi, M. Eftekhari, and H. Ghalkhani. 2012. "Combining Optical and Thermal Remote Sensing Data for Mapping Debris-Covered Glaciers (Alamkouh Glaciers, Iran)." *Cold Regions Science and Technology* 71: 73–83. doi:10.1016/j.coldregions.2011.10.004.

Keshri, A. K., A. Shukla, and R. P. Gupta. 2009. "ASTER Ratio Indices for Supraglacial Terrain Mapping." *International Journal of Remote Sensing* 30 (2): 519–524. doi:10.1080/01431160802385459.

Lemke, P., J. Ren, R. Alley, I. Allison, J. Carrasco, G. Flato, Y. Fujii, et al. 2007. *Observations: Change in Snow, Ice and Frozen Ground. Climate Change 2007: The Physical Science Basis*, 337–384. Edited by S. Solomon, D. Qin, M. Manning, Z. Chen, M. Marquis, K. B. Averyt, M. Tignor, and H. L. Miller Contribution of Working Group I to the Fourth Assessment Report of the intergovernmental panel on climate change. Cambridge: Cambridge University Press.

Liu, Q., C. Mayer, and S. Liu. 2013. "Distribution and Recent Variations of Supraglacial Lakes on Dendritic-Type Glaciers in the Khan Tengri-Tomur Mountains, Central Asia." *The Cryosphere Discussions* 7: 4545–4584. doi:10.5194/tcd-7-4545-2013.

Liu, S. Y., X. J. Yao, W. Q. Guo, J. L. Xu, D. H. Shangguan, J. F. Wei, W. J. Bao, and L. Z. Wu. 2015. "The Contemporary Glaciers in China Based on the Second Chinese Glacier Inventory." *Acta Geographica Sinica* 70 (1): 3–16. doi:10.11821/dlxb201501001.

Meier, M. F. 1980. "Remote Sensing of Snow and Ice/La Télédétection De Neige Et De Glace." *Hydrological Sciences Bulletin* 25 (3): 307–330. doi:10.1080/02626668009491937.

Paul, F., N. E. Barrand, S. Baumann, E. Berthier, T. Bolch, K. Casey, H. Frey, et al. 2013. "On the Accuracy of Glacier Outlines Derived from Remote-Sensing Data." *Annals of Glaciology* 54 (63): 171–182. doi:10.3189/2013AoG63A296.

Paul, F., C. Huggel, and A. Kääb. 2004. "Combining Satellite Multispectral Image Data and a Digital Elevation Model for Mapping Debris-Covered Glaciers." *Remote Sensing of Environment* 89: 510–518. doi:10.1016/j.rse.2003.11.007.

Paul, F., A. Kääb, M. Maisch, T. Kellenberger, and W. Haeberli. 2002. "The New Remote-Sensing-Derived Swiss Glacier Inventory: I. Methods." *Annals of Glaciology* 34 (1): 355–361. doi:10.3189/172756402781817941.

Pfeffer, W. T., A. A. Arendt, A. Bliss, T. Bolch, J. G. Cogley, A. S. Gardner, J.-O. Hagen, et al. 2014. "The Randolph Glacier Inventory: A Globally Complete Inventory of Glaciers." *Journal of Glaciology* 60: 537–552. doi:10.3189/2014JoG13J176.

Racoviteanu, A. E., F. Paul, B. Raup, S. J. S. Khalsa, and R. Armstrong. 2009. "Challenges and Recommendations in Mapping of Glacier Parameters from Space: Results of the 2008 Global Land Ice Measurements from Space (GLIMS) Workshop, Boulder, Colorado, USA." *Annals of Glaciology* 50 (53): 53–69. doi:10.3189/172756410790595804.

Ranzi, R., G. Grossi, L. Iacovelli, and S. Taschner. 2004. "Use of Multispectral ASTER Images for Mapping Debris-Covered Glaciers within the GLIMS Project." *Proceedings of the IEEE International Geoscience and Remote Sensing Symposium, IGARSS '04* 2: 1144–1147.

Shen, J. 2003. "The Climbing Yengisogat Range in the Chinese Karakoram." http://www.summitpost.org/mount-crown-huangguan/152162

Shi, Y., C. Liu, and Z. Wang, eds. 2008. *Concise Glacier Inventory of China*, 65–71. Shanghai: Shanghai Popular Science Press.

Short Sr., N. M. 1999. "The Remote Sensing Tutorial: Section 1. Contrast Stretching and Density Slicing." Online tutorial book. http://www.fas.org/irp/imint/docs/rst/Sect1/Sect1_12a.html

Shukla, A., M. K. Arora, and R. P. Gupta. 2010. "Synergistic Approach for Mapping Debris-Covered Glaciers Using Optical-Thermal Remote Sensing Data with Inputs from Geomorphometric Parameters." *Remote Sensing of Environment* 114: 1378–1387. doi:10.1016/j.rse.2010.01.015.

Shukla, A., R. Gupta, and M. K. Arora. 2010. "Delineation of Debris-Covered Glacier Boundaries Using Optical and Thermal Remote Sensing Data." *Remote Sensing Letters* 1 (1): 11–17. doi:10.1080/01431160903159316.

Silverio, W., and J.-M. Jaquet. 2005. "Glacial Cover Mapping (1987 – 1996) of the Cordillera Blanca (Peru) Using Satellite Imagery." *Remote Sensing of Environment* 95 (3): 342–350. doi:10.1016/j.rse.2004.12.012.

Taschner, S., and R. Ranzi. 2002. "Comparing the Opportunities of Landsat-Tm and ASTER Data for Monitoring a Debris Covered Glacier in the Italian Alps within the GLIMS Project." *Proceedings of the IEEE International Geoscience and Remote Sensing Symposium, IGARSS '02* 2: 1044–1046.